Tellus (2001), 53A, 56–73

TELLUS
ISSN 0280–6495

Toward a phase-space cartography of the short- and medium-range predictability of weather regimes

By S. VANNITSEM*, *Institut Royal Météorologique de Belgique, Avenue Circulaire, 3, 1180 Bruxelles, Belgium*

(Manuscript received 27 December 1999; in final form 13 June 2000)

ABSTRACT

We compare the short- and medium-range predictability of weather regimes of a quasi-geostrophic model as defined by a hierarchical cluster algorithm and a Lyapunov-based clustering method recently introduced in the literature. Both procedures lead to weather regimes displaying very different predictability properties on the short and medium range bases. While the former does not distinguish between stable and unstable weather regimes, the latter leads to clusters which do not display a good medium range predictability. We introduce a new clustering method taking advantages of the two previous techniques. Its application in the context of the quasi-geostrophic model gives rise to regimes possessing at the same time a good medium range skill and well separated instability properties, indicating the possibility to build a systematic cartography of the short-term predictability of weather fields in phase space.

1. Introduction

The ultimate goal of meteorology is to provide reliable forecasts for the evolution of the atmospheric fields. The main difficulty in this perspective is the natural unpredictability of the flow beyond a certain time interval whose origin is found in the intrinsic property of sensitivity to initial conditions. Nowadays, major efforts are devoted to the analysis of this property which is most naturally tackled in the context of chaos theory (Ott, 1993). In this framework, the way to predict the evolution of a system is conditioned essentially by the time scale for which the forecast is desired. If one is interested in the short term evolution of the system, a reliable deterministic prediction starting from the dynamical equations can be performed up to a time of the order of $1/\sigma_{\max} \ln(1/\varepsilon)$ where $\sigma_{\max}$ is the dominant Lyapunov exponent and ε a sufficiently small error associated to the initial condition. Beyond this time, the error behaves essentially in an erratic way thanks to the nonlinearities of the system and one must therefore resort to a probabilistic approach (Nicolis and Nicolis, 1995).

The probabilistic approach is being adopted nowadays in several meteorological centers and relies on the integrations of the operational weather prediction model starting from an ensemble of closely lying initial conditions (Molteni et al., 1996; Toth and Kalnay, 1997). However, because of the large number of variables involved the size of the ensemble considered in their statistical description is quite small. As a result the predictive skill of the approach followed is highly dependent on the number of integration performed. To circumvent this difficulty, an alternative approach is to classify beforehand weather situations as a function of their predictability properties and to give in that way a cartography of their dynamical properties in phase space.

Several works have analyzed the predictability properties of weather situations pertaining to particular regimes such as the PNA pattern (Palmer,

* e-mail:svn@oma.be

1988; Hannachi, 1997; Corti and Palmer, 1997) or zonal and blocking situations (Legras and Ghil, 1985; Kimoto et al., 1992; Colucci and Baumhefner, 1992; Frederiksen, 1997). But they did not give a full picture of the predictability properties of weather situations in phase space.

A first analysis toward such a description has been performed by Trevisan (1995) who investigates the predictability properties of weather regimes as defined by a hierarchical cluster algorithm (HCA). The author shows that all the weather regimes defined in this way display a similar short-term predictability, while on a medium range basis they keep useful information (better than the climatological prediction) beyond 10 days, indicating their potential use for prediction. It seems therefore that this algorithm (HCA) based essentially on the location of the fields in phase space is not optimal to classify the fields in terms of their short-term predictability.

In the present paper, we develop a clustering method enabling for a systematic classification of weather fields in terms of their short-term predictability properties. It is based on a combination of the HCA procedure and an approach recently proposed by Vannitsem and Nicolis (1998) which consists to cluster the weather fields on the basis of their dynamical properties such as the local Lyapunov exponents (LA). As it will turn out, its application in the context of a simple QG model (Marshall and Molteni, 1993) allows for a systematic cartography of the instability in phase space.

In Section 2, we present shortly the model. Sections 3 and 4 are then devoted to the analysis of short and medium range predictability of weather regimes as defined by the HCA and the LA procedures, respectively. Both procedures lead to weather regimes displaying very different predictability properties on the short and medium range bases. While the former does not distinguish between stable and unstable weather regimes, the latter leads to clusters which do not display a good medium range predictability. We have therefore developed a new clustering method taking advantages of the two previous techniques (Section 5) which leads to weather regimes displaying well separated instability properties and a good medium range skill. Finally in Section 6, we draw our conclusions.

2. The T21 quasi-geostrophic atmospheric model

The exhaustive evaluation of the dynamical properties of operational atmospheric models is drastically limited by the computer power available. Such an analysis can therefore only be performed on simplified models designed to describe some specific features of the atmosphere. In our study, we use a 3-level global quasi-geostrophic spectral model (QG model) which was built in order to represent the dynamics of the largest scale of the atmosphere at middle latitudes. In this section, we present shortly the model equations and some of its dynamical properties.

The model describes the evolution of the potential vorticity at 200 hPa, 500 hPa and 800 hPa (Marshall and Molteni, 1993). The horizontal fields Z are expanded in series of spherical harmonics $Y_{m,n}$ truncated triangularly at wavenumber 21:

$$Z(\lambda, \phi, t) = \sum_{n=0}^{21} \sum_{m=-n}^{m=n} Z_{m,n}(t) Y_{m,n}(\lambda, \phi), \tag{1}$$

where λ, ϕ, m and n are the longitude, the latitude, the zonal and total wavenumbers, respectively. The index n represents a total (two-dimensional) wavenumber on the sphere and characterizes the size of the two-dimensional horizontal structures. The prognostic equation at each level, i, can then be written in terms of the streamfunction ψ and the potential vorticity q as

$$\frac{\partial q_i}{\partial t} = -J(\psi_i, q_i) - D(\psi_i) + S_i, \tag{2}$$

where J is the jacobian of the two-dimensional field. The linear term D accounts for the effects of Newtonian relaxation of temperature, a scale selective horizontal diffusion of vorticity and temperature and a drag on the 800 hPa wind whose coefficient depends on the properties of the underlying surface. The damping time scale τ_d at total wavenumber 21 associated to the horizontal diffusion was fixed in Marshall and Molteni (1993) to 2 days. Finally the time-independent spatially varying source term, S, constrains the solution of the model to an averaged, statistically stable, observed winter climatology ("perpetual winter" conditions). Note that all the fields are computed in nondimensional units: the length unit is the earth radius (6371 km) and the time unit is half the inverse of the angular velocity of the earth ($7.292 \times 10^{-5}\ s^{-1}$). The model equations are integrated in time using a leapfrog scheme for the Jacobian term, J, and a forward scheme for the linear operator, D, with a time step of 1 h.

The dynamics of this model has been investigated in details in Vannitsem and Nicolis (1997). It was shown that the solution of model (2) is chaotic and lives on a high-dimensional attractor. The largest Lyapunov exponent and the Kolmogorov–Sinai entropy are equal to $0.23\ \mathrm{day}^{-1}$ and $7.3\ \mathrm{day}^{-1}$, respectively. The details of the computation are given in the Section 8. We represent in Fig. 1 the Lyapunov spectrum up to the 400th exponent obtained after an integration period of 1000 days.

We have also evaluated the local values of these exponents for a period of 50,000 days (about 600 winters). Due to the large computer demand for the computation of the local Lyapunov exponents, we limit ourselves to the 20 dominant ones and fix $L^+ = 20$ in (A.10). Figs. 2a, b display respectively a portion of the evolution of the local values of the largest exponent and of the local K-entropy along the trajectory of the solution. We observe a clearcut non-uniform character of these properties on the attractor suggesting the possibility of finding global weather situations (clusters) which display differential instability properties. This aspect is first investigated in the next section through the inspection of the predictability of clusters defined using the hierarchical cluster algorithm (HCA).

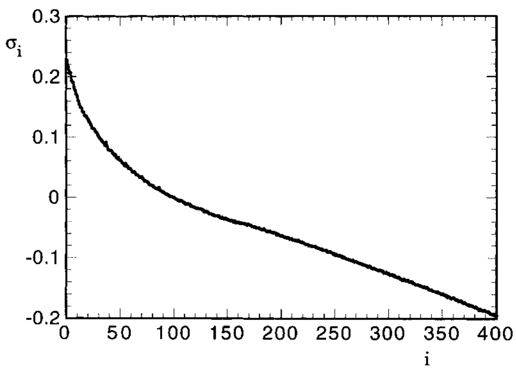

Fig. 1. The Lyapunov spectrum up to the 400th exponent of model (2) as obtained after 1000 days of integration. σ_i is the value of ith exponent.

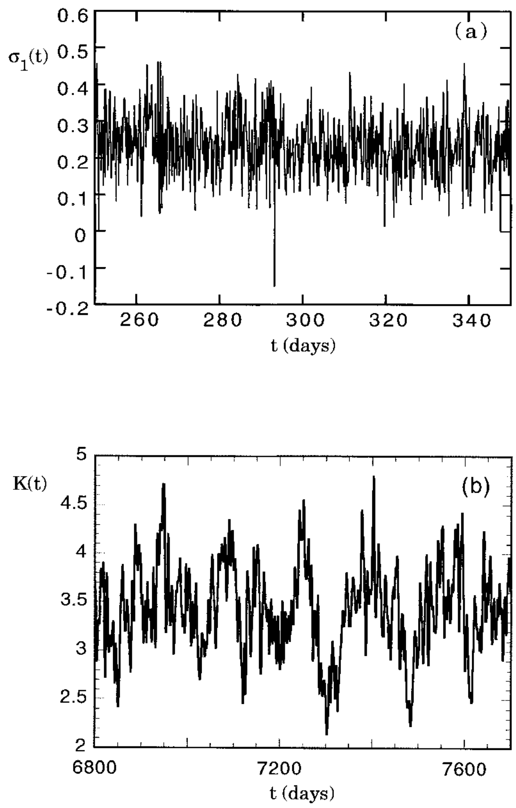

Fig. 2. (a) Time evolution of the 1st local Lyapunov exponents, eq. (A.7), and (b) of the local K-entropy, eq. (A.10).

3. Short and medium range predictability of HCA weather regimes

One objective method to classify weather fields in different regimes is the hierarchical cluster algorithm (Ward, 1963) which was used by Cheng and Wallace (1993) and Trevisan (1995) on real data sets. This technique consists mainly to assemble close weather fields in phase space. It can be performed directly in the phase space defined by the ensemble of the variables of the system, such as the spectral modes of the different atmospheric fields. But, one of the most popular approaches consists to expand the meteorological fields in an orthogonal basis and to perform the cluster analysis in the phase space defined by the dominant components of the field in this basis. One of them is given by the eigenvectors of the covariance matrix of the fields, known as the principal components or the Empirical Orthogonal Functions (EOFs).

Cheng and Wallace (1993) used this technique for a large dataset of 40 winters in both the full phase space and the EOFs space. They have isolated three dominant (and robust) clusters, named "Alaska Ridge" (A), "Greenland blocking" (G) and "Rockies ridge" (R) regimes, which are respectively marked by a ridge over the gulf of Alaska, by a closed anticyclone over the southern tip of Greenland and by a ridge over the Rockies. The A and R regimes for the north Pacific sector resemble to the opposite Pacific North Atlantic patterns (PNA) and the third cluster G resembles in the north Atlantic sector to the North Atlantic Oscillation pattern already found in other studies (Wallace and Gutzler, 1981; Barnston and Livezey, 1987). Moreover, they have shown that these patterns are very similar to the ones found in the space of the leading EOFs.

Similar results have been obtained by Trevisan (1995) using a real data set of 35 winters. She classified the daily fields in 5 clusters using the hierarchical algorithm and she identified the three regimes defined by Cheng and Wallace (1993) referred in Trevisan's work as PNA, BNAO and RNA patterns together with two zonal regimes, ZNAO1 and ZNAO2.

We have performed a similar five-cluster analysis of 2000 daily fields at the 500 hPa level generated from the QG3 model (about 22 winters). Fig. 3 displays the centroids (defined as the average of the fields belonging to that cluster) of these clusters. As expected the clusters obtained in this model do not match perfectly the ones obtained from real data but show strong similarities. The second cluster possesses a strong ridge over eastern pacific suggesting that it corresponds to weather situations having a significant projection on the negative PNA pattern (RNA). While the fourth cluster displays a ridge over the Rockies and a zonal flow over the eastern pacific indicating a significant projection on the positive PNA pattern. The fifth cluster correponds to the ZNAO1 pattern of Trevisan (1995) displaying a positive anomaly over eastern pacific and Europe. While the third cluster corresponds to the ZNAO2 pattern. Finally, the first cluster resembles the BNAO pattern (or G in Cheng and Wallace, 1993).

If one reduces further the number of clusters to 3, the third and fifth clusters and the first and fourth ones collapse. Fig. 4 displays the centroids of these new clusters. For this new system, the 1st and 3rd clusters show approximately opposite anomalies whereas the second is still representative of the negative PNA pattern.

As indicated in the Introduction, the short range predictability of weather fields can be fully characterized by the evaluation of the Lyapunov exponents. On longer time scales, the evaluation of the predictability is complicated by the probabilistic nature of the dynamics. Legras and Ghil (1985) have proposed to evaluate the medium range predictability of weather situations using their persistence around a particular weather regime. They called this approach *regime predictability*. However, the persistence does not fully characterize the medium range predictability of weather situations since weather fields can experience successive transitions from one regime to another which are still predictable in a statistical sense (Nicolis et al., 1997). One must therefore resort to alternative tools such as the ones provided by the Information Theory to get the full characterization of the medium range predictability (Lasota and Mackey, 1995). This approach adopted throughout the paper is described in Subsection (3.2).

3.1. Short range predictability

Corti and Palmer (1997) suggested that clusters showing negative PNA patterns are more sensitive to perturbations than other fields. In order to check this we have computed for each cluster the average Lyapunov exponent and the average K-entropy defined respectively as:

$$\overline{\lambda_1^{\mathrm{C}}} = \int_{\boldsymbol{X} \in C} \lambda_1(\boldsymbol{X}) \rho(\boldsymbol{X})\, \mathrm{d}\boldsymbol{X}, \tag{3}$$

$$\overline{K^{\mathrm{C}}} = \int_{\boldsymbol{X} \in C} K(\boldsymbol{X}) \rho(\boldsymbol{X})\, \mathrm{d}\boldsymbol{X}, \tag{4}$$

where $\rho(\boldsymbol{X})$ is the invariant probability distribution and C is the cluster at hand. The results are given in Table 1.

One observes that the average Lyapunov exponent resulting from the analysis does not allow to isolate high or low predictability weather regimes in a clearcut manner. This result is consistent with the one presented in Lin and Derome (1996) who studied the predictability properties of positive

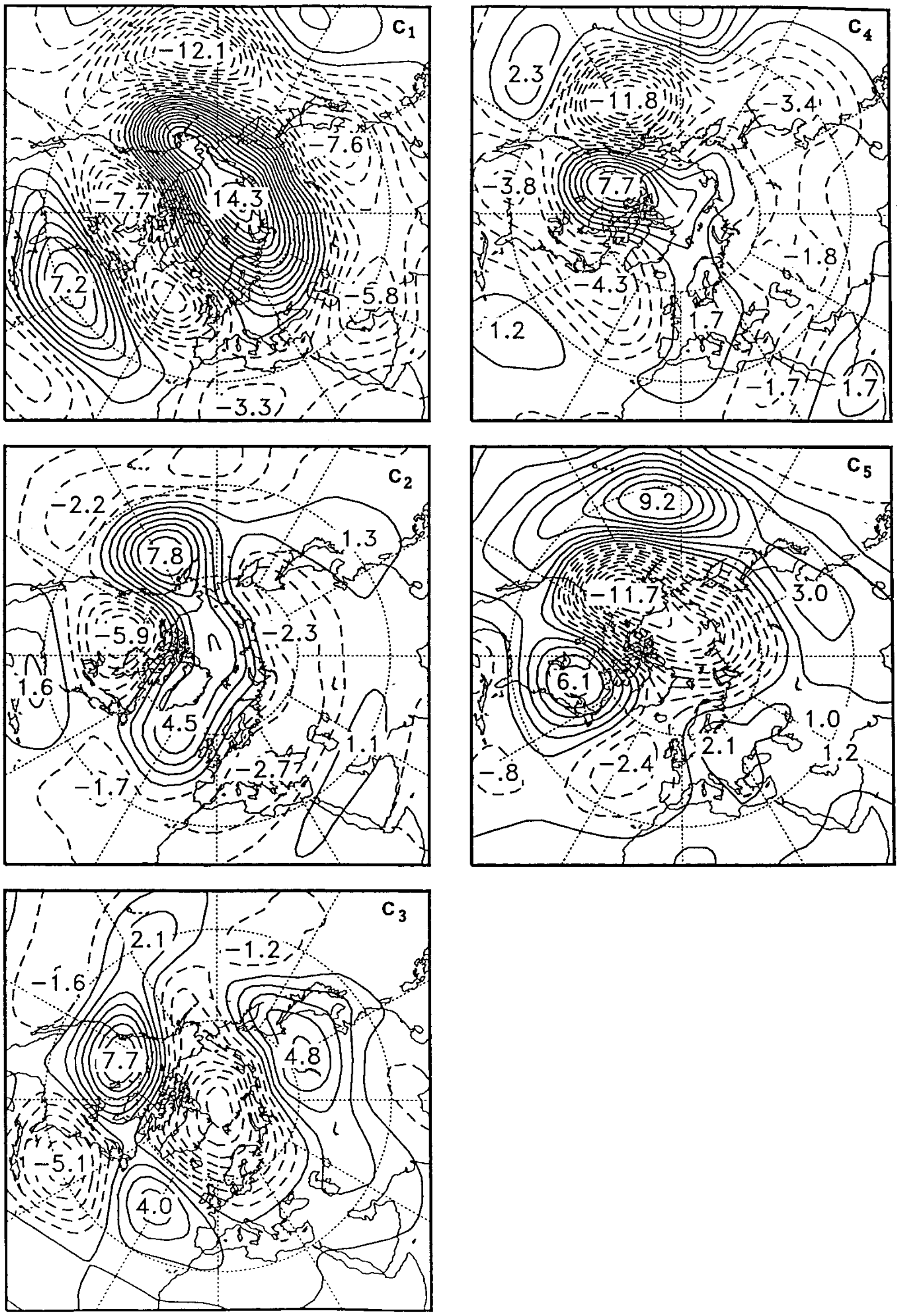

Fig. 3. Mean field anomaly ($10^6\ m^2/s$) of the 5-cluster classification based on the Hierarchical Cluster Algorithm using 2000 daily fields. C_1 to C_5 are respectively plotted from the upper left to the bottom right.

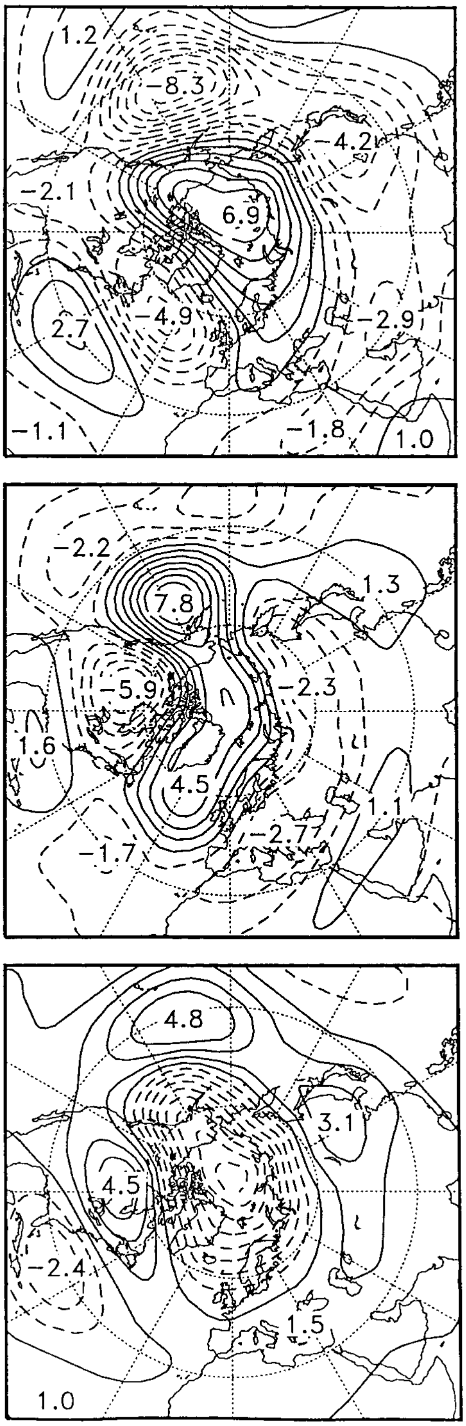

Fig. 4. Mean field anomaly ($10^6\,m^2/s$) of the 3-cluster classification based on the hierarchical cluster algorithm using 2000 daily fields. C_1 to C_3 are respectively plotted from the top to the bottom.

and negative PNA patterns in the QG model and who showed that the initial mean error behavior of both patterns is similar.

Therefore, in order to isolate highly predictable regimes, one must resort to an alternative classification technique allowing for such a distinction. This approach will be presented in Section 4.

3.2. Medium range predictability

As stressed in Section 1, the probabilistic prediction in the full phase space of the continuous atmospheric model constitutes an heavy task on both the computer power side and the subsequent construction of the probability densities. Instead, one can envisage to perform this prediction in the discrete state space system defined by the weather regimes, remembering that these coarse-grained weather situations potentially contain large-scale information which can be predicted for long times (Molteni et al., 1990; Trevisan, 1995). Let us investigate from this point of view the medium range predictability of the 3-cluster system.

In this context, it is usually assumed that the process is first order Markov (Fraedrich and Müller, 1982; Spekät et al., 1983; Hannachi and Legras, 1995). This implies that the evolution of the system is fully defined once one specifies the transition probability matrix, $\boldsymbol{W}$. Each entry of this matrix, W_{ij}, represents the probability to perform a transition to state j at time $t=(n+1)\Delta t$ starting from state i at time $t=n\Delta t$ where Δt is the time step between successive events in the series generated by the model. These entries are normalized in such a way that $\sum_j W_{ij}=1$.

For the 3-cluster system of Fig. 4, this matrix computed from a series of 400,000 data points sampled every 3 hours reads

$$W=\begin{pmatrix} 0.982 & 0.010 & 0.008 \\ 0.016 & 0.970 & 0.014 \\ 0.004 & 0.010 & 0.986 \end{pmatrix} \tag{5}$$

From this matrix, one can already note that the probabilities to stay in a particular regime is high,

Table 1. *Cluster-averaged Lyapunov exponent and K-entropy for the 5-cluster (left) and 3-cluster (right) systems*

Cluster	λ_1^C	K^C	Nb members	Cluster	λ_1^C	K^C	Nb members
1	0.245	3.50	218	1	0.235	3.41	593
2	0.229	3.47	582	2	0.229	3.47	582
3	0.223	3.45	444	3	0.225	3.42	825
4	0.225	3.35	375				
5	0.227	3.38	381				

indicating the important persistence of the system along the different regimes. This characteristic is further illustrated by computing the escape time probability which is defined as the probability to leave a particular state after a certain time n, $F(C_j, 0; \overline{C_j}, t=n\Delta t)$, or more explicitely,

$$P(x_1 \in C_j;\ x_2 \in C_j;\ \dots;\ x_{n-1} \in C_j;\ x_n \in \overline{C_j}),$$

where $x_1, x_2, \dots, x_n$ are the successive states visited by the system during the period $t=n\Delta t$ and $\overline{C_j}$ is the complement of C_j. This quantity has been computed for our 3-state system and is shown in Fig. 5. For reference, we have plotted the escape time probability assuming that the dynamics is Markovian,

$$F(C_j, 0; \overline{C_j}, t) = (W_{ij})^{n-1} - (W_{jj})^n, \tag{6}$$

where the W_{jj} are the entries on the diagonal of the transition matrix (5). The slow decreasing shape of this quantity indicates that the system can persist for long times along a particular cluster, the least persistent one being the second cluster. Moreover, there is a discrepancy between the predicted value assuming that the process is Markovian and the actual escape time probability distributions. This difference is substantial for C_1 and C_3 and can attain a factor of the order of 2 for long escape times. However, the agreement is relatively good for C_2 up to about 10 days.

From a practical point of view, one is usually interested not only to predict the persistence in a particular weather regime but also to predict the probability to be in a state j at time t starting from a particular state i at time $t=0$. To quantify this probabilistic evolution, one can explore the dynamics in terms of information theory. A central quantity of this theory is the *Shannon entropy* defined as

$$S(C_i, t) = -\sum_{C_j} P(C_j, t \mid C_i, 0) \ln[P(C_j, t \mid C_i, 0)], \tag{7}$$

which allows to measure the amount of information needed to localize the system in a particular state j at a given time t starting from state i (Lasota and MacKey, 1995). The evolution in time of this quantity gives an indication on how fast the system spreads in the state space. As time evolves, this quantity converges to a constant whose value depends on the asymptotic probabilities, $P_\infty(C_j)$. Another natural measure of the convergence to the asymptotic probabilities is given by the conditional entropy which uses the asymptotic probability as a reference,

$$E_{\mathrm{kul}}(C_i, t) = \sum_{C_j} P(C_j, t \mid C_i, 0) \ln\left(\frac{P(C_j, t \mid C_i, 0)}{P_\infty(C_j)}\right), \tag{8}$$

which is known as the *Kullback entropy*. Fig. 6 shows (8) for the 3-cluster system. For reference we have drawn in the same figure the evolution of E_{kul} when the process is first order Markov with a transition probability matrix given by eq. (5), where the instantaneous probabilities $P(C_j, t \mid C_i, 0)$ can be calculated explicitly from the Chapman–Kolmogorov equation (Feller, 1967),

$$\boldsymbol{p}(t) = \boldsymbol{p}(0)\boldsymbol{T}^n \tag{9}$$

where $\boldsymbol{p}(t) = [p_{C_1}(t), \dots, p_{C_S}(t)]$ is the (vector) probability to be in a particular state C_j for $j = 1, \dots, S$ at time $t = n\Delta t$ and the stochastic matrix $\boldsymbol{T}^n$ is given by

$$(\boldsymbol{T}^n)_{j,k} = \sum_{\alpha=1}^{3} G_\alpha v_j^{(\alpha)} u_k^{(\alpha)} \lambda_\alpha^n, \tag{10}$$

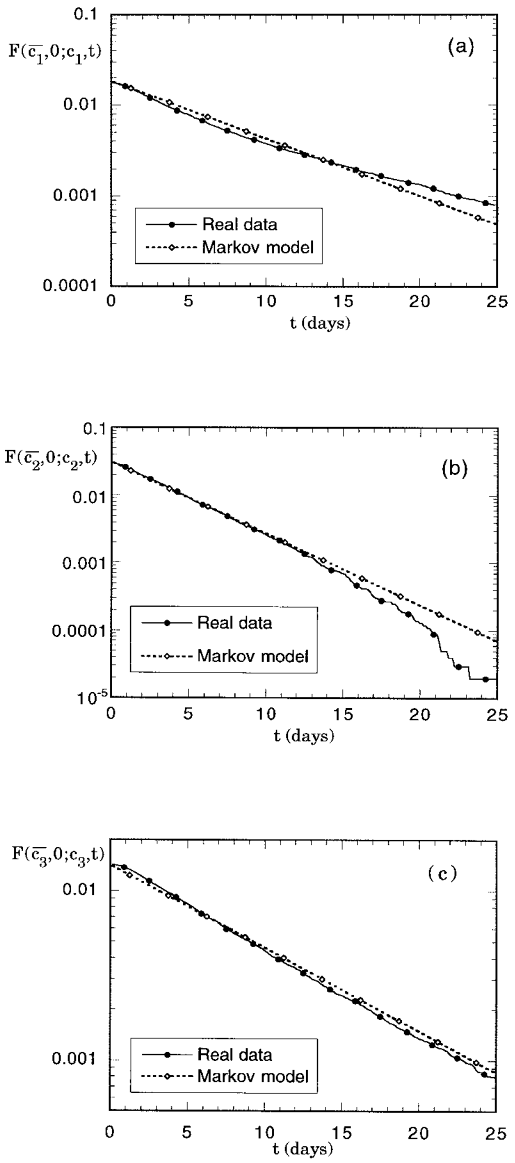

Fig. 5. Evolution of the escape time probability (dots) for cluster C_1, (a), C_2, (b), and C_3, (c), as obtained from a series of 400,000 data points sampled every 3 h. For reference, we have drawn the escape time probability obtained assuming that the system is Markovian (squares).

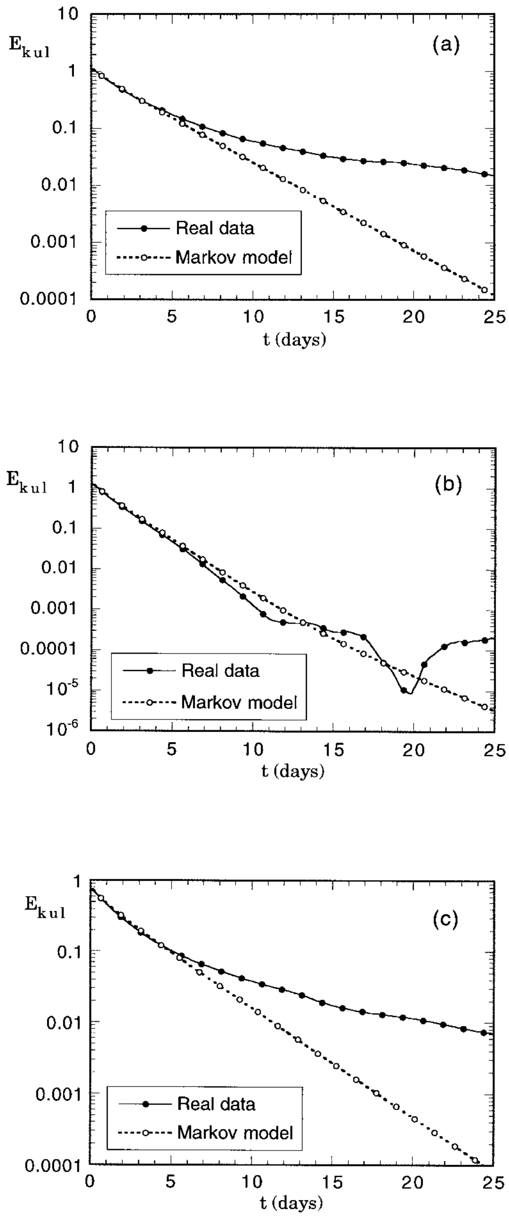

Fig. 6. Evolution of the Kullback entropy (filled dots) for cluster C_1, (a), C_2, (b), and C_3, (c), as obtained from a series of 400,000 data points sampled every 3 h. For reference, we have drawn the E_{kul} obtained assuming that the system is Markovian (open dots).

where $\boldsymbol{u}^{(\alpha)}$ are the right eigenvectors of the transition matrix $\boldsymbol{W}$, $\boldsymbol{v}^{(\alpha)}$, the left eigenvectors and λ^{α}, the eigenvalues. The parameters G_{α} are determined by the biorthonormalisation condition

$$G_\alpha \sum_{k=1}^{3} v_k^{(\alpha)} u_k^{(\alpha)} = 1. \tag{11}$$

The behavior of E_{kul} displays a slow decrease beyond 1 week for clusters C_1 and C_3, indicating that the system keeps information for long times which is better than the simple prediction based on the asymptotic probabilities. For cluster C_2, the decrease is faster and E_{kul} converges to its asymptotic value (0) after about 15 days. The negative PNA pattern is therefore less predictable than the two other clusters on a long term basis. This result is consistent with the one found by Trevisan (1995) who shows that the prediction starting from this cluster degrades more rapidly than for other weather regimes. Notice that the non-Markovian character is even more evident suggesting that long term memory effects are acting on the dynamics.

In summary, one must stress that there is an important difference between the short and medium range predictability of these clusters. On a short term basis, they all have the same predictability limit as defined by the Lyapunov exponents but the fields starting from C_2 spreads out much faster over the whole state space than from the other clusters. Using this classical technique, one can discriminate weather situations which keep useful information in the medium range but one cannot infer anything about their short term properties. One must therefore resort to another classification designed precisely to this aim.

4. Short and medium range predictability of LA clusters

Recently, a novel approach of clustering has been proposed based solely on intrinsic properties of the system such as the Lyapunov exponents (Vannitsem and Nicolis, 1998). In the present section, we generalize this approach by constructing weather clusters using a local volume expansion rate. Here the separation of clusters is performed by collecting fields having close instability properties as measured by the local Lyapunov exponent or by the local K-entropy (Section 8). This allows one to isolate the stable and unstable situations, or in other words to know in advance the short-term predictability properties of particular weather fields.

4.1. The short-term predictability

We can first look for weather patterns separated by given thresholds of the local Lyapunov exponents whose maximum and minimum values fix the upper and lower limits of the possible thresholds. These extremes are equal to 0.83 and -0.15, respectively. One therefore fixes the threshold values to 0.4 day^{-1} and to 0.1 day^{-1} (see Fig. 2a). This allows to separate weather fields in three categories for which the dominant Lyapunov exponents lie in the ranges $L_1 = [-\infty, 0.1[$, $L_2 = [0.1, 0.4]$, and, $L_3 =]0.4, \infty]$. This particular procedure does not a priori yield to weather clusters well separated in phase space such as the ones obtained through the Ward's method but should give important information on the dynamical instability of the weather fields. Notice that if weather patterns are perfectly independent of the instability properties of the field as measured by the Lyapunov exponents, then the centroids of these two clusters would be close to the climatological average (anomalies close to 0).

Figs. 7a, c show the centroids at 500 hPa associated to the first and third clusters (see also Vannitsem and Nicolis (1998)). The 2nd cluster is not shown since its centroid is very close to the climatology. A clear tendency is present. For large values of the dominant Lyapunov exponent, the centroid displays positive anomalies over eastern and south western pacific, on Siberian regions, on the atlantic and central America. While for small values, the situation is roughly the opposite with positive anomalies over the Rockies, Europe and on central pacific and Atlantic. The former seems therefore to be close to the negative PNA situation as defined by Molteni and Palmer (1993) for this model while the latter to the positive PNA pattern.

The specific choice of the limits of the different categories presented above is quite arbitrary. If now we displace the threshold ranges to $L_1 = [-\infty, 0.05[$, $L_2 = [0.05, 0.45]$, and, $L_3 =]0.45, \infty]$, the anomalies are even stronger (Figs. 7b, d). This suggests that the larger (smaller) is the value of the dominant local Lyapunov exponents, the larger (the smaller) are the anomalies of the centroids.

In phase space, the error dynamics is not only

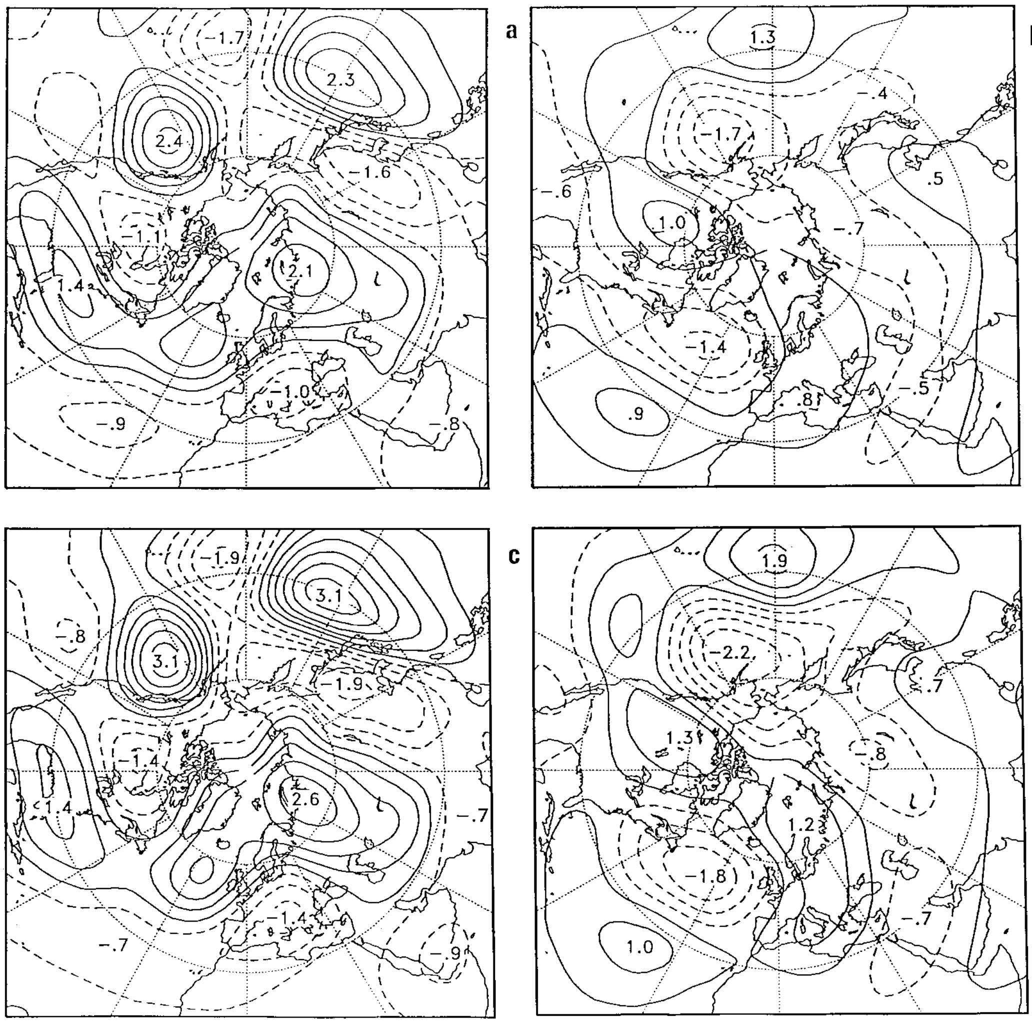

Fig. 7. Mean field anomaly (10^6 m^2/s) associated to local amplification rates of the dominant Lyapunov vector larger than 0.4 day^{-1}, (a), smaller than 0.1 day^{-1}, (b), larger than 0.45 day^{-1}, (c), and smaller than 0.05 day^{-1}, (d), obtained after an integration of 20,000 days.

managed by the largest Lyapunov exponent but by the whole spectrum of positive Lyapunov exponents which is measured by the K-entropy (see Section 8). We therefore perform a similar clustering procedure using the K-entropy defined by eq. (A.10), keeping in mind that the maximum and minimum values recorded for our QG model are equal to 5.85 and 1.88. To this end, we separate weather patterns according to the ranges of K-entropy values $L_1 = [-\infty, 2.5[$, $L_2 = [2.5, 4.0]$, and, $L_3 =]4.0, \infty]$. Figs. 8a, b show the centroids of clusters L_1 and L_3. We are now faced with two opposite patterns with even stronger anomalies than the ones found using only the dominant Lyapunov exponent. As for the previous analysis, it is clear that the centroid corresponding to large values of the K-entropy (Fig. 8a) possess a clear negative PNA pattern while the second (Fig. 8b) presents the signature of the positive PNA pattern. Note that the stable cluster (positive PNA) found using the K-entropy is close to the one obtained using only the first local Lyapunov exponent. This

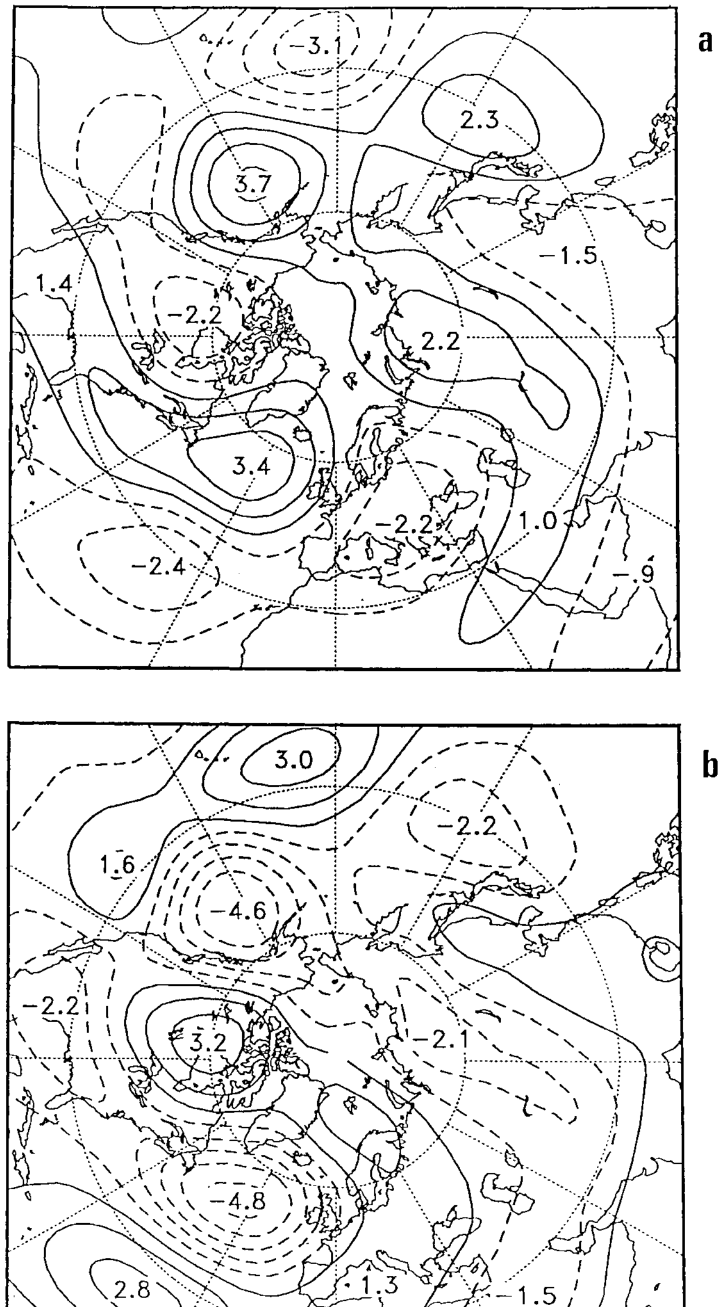

Fig. 8. Mean field anomaly ($10^6\ m^2/s$) associated to local *K*-entropy larger than $4.0\ day^{-1}$, (a), and smaller than $2.5\ day^{-1}$, (b).

suggests that a stable regime as defined by the dominant Lyapunov vector is also a stable situation in the 20-dimensional subspace spanned by the 20 dominant Lyapunov vectors.

Fig. 9 displays the projection of 500 hPa-fields on the axis defined by the difference between the centroids of the two clusters presented in Figs 8a, b as a function of the K-entropy values associated to these fields. The projection along this axis constitutes in some sense an index for the strength of the PNA pattern. Although the variability of the K-entropy values is quite large for a particular projection along this axis, there is a clear tendency to have high K-entropy values for large positive projections and low K-entropy values for large negative projections. Déqué (1988) has also isolated a particular predictable axis for the ECMWF model through the minimisation of the error made during the whole forecast period. The spatial patterns presented in Fig. 8a shows strong similarities with the ones found by Déqué except that the Euro-atlantic pattern is shifted westward. This westward shift of the anomaly pattern over the Atlantic can be related to the deficiencies of the model (Corti and Palmer, 1997).

4.2. The medium range predictability

The original fine-scaled dynamics generated by model (2) is now mapped into a symbolic dynamics associated with the succession of 3 symbols — the low, medium and high predictability regimes. As in the previous section, we construct the transition matrix which takes the explicit form:

$$W = \begin{pmatrix} 0.8321 & 0.1679 & 0 \\ 0.0101 & 0.9886 & 0.0013 \\ 0 & 0.102 & 0.898 \end{pmatrix}. \qquad (12)$$

One first notes that two entries of this matrix are equal to 0, reducing in that way the number of possible transitions which can occur in the system. However, the probability to stay in states L_1 and L_3 are smaller than the ones given in the previous clustering method (HCA), implying that the system will not persist for long times around these clusters and will loose rapidly information on its localization in state space. This behavior is further substantiated in Fig. 10 where we represent the Kullback entropy for this 3-state system. Indeed, one observes that the entropy decreases rapidly at the beginning indicating the rapid transition to the other clusters. After about 2 days, the variation of E_{kul} slows down and continues to decrease up to 15 days, indicating that the system keeps useful information up to 15 days. For reference we have also drawn E_{kul} under the Markov assumption. The discrepancy between the reality and the Markov process is now very large suggesting that

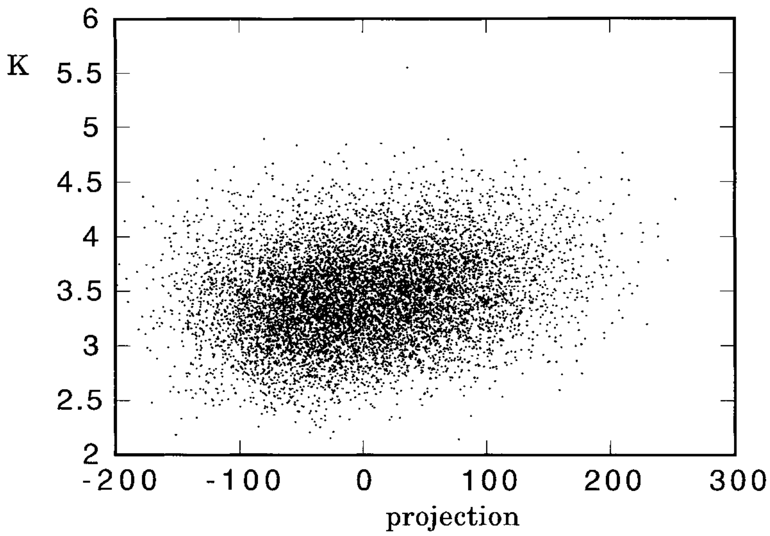

Fig. 9. The local K-entropy, eq. (A.10), as a function of the projection along the axis defined by the difference between the centroids of Fig. 8.

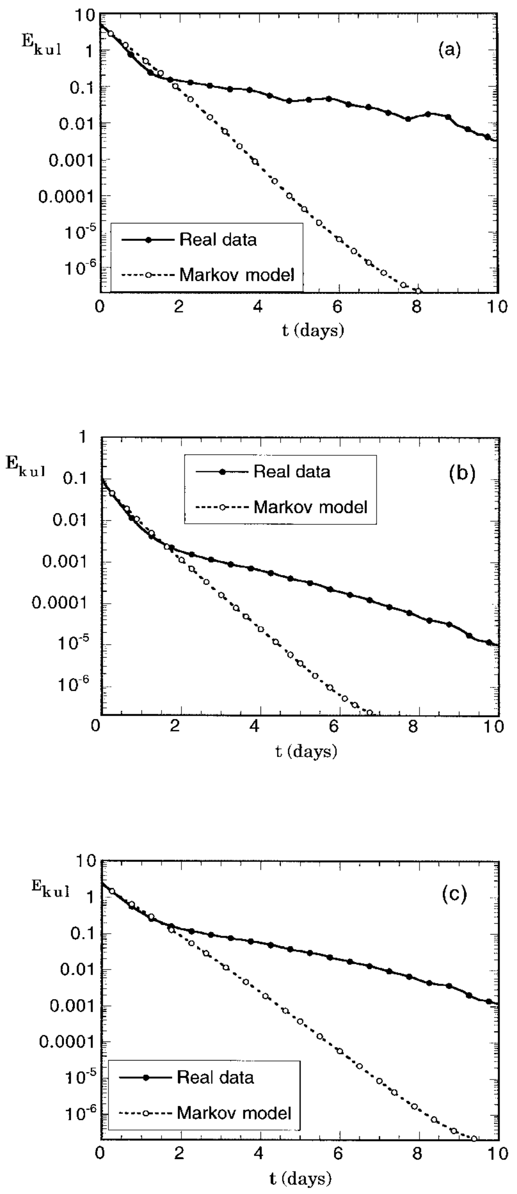

Fig. 10. Evolution of the Kullback entropy (filled dots) for the cluster L_1, (a), L_2, (b), and L_3, (c), as obtained from a series of 400,000 data points sampled every 3 h. For reference, we have drawn the E_{kul} obtained assuming that the system is Markovian (open dots).

the modelling of the process at hand cannot be based on the Markovian assumption. One must therefore resort to another modelling starting from the full set of joint probabilities $P(x_1, x_2, \ldots, x_n)$ where $x_1, x_2, \ldots, x_n$ are the successive states visited by the system (Nicolis et al., 1997).

In summary, although the Lyapunov-based clustering procedure indicates a clearcut short time scale predictability tendency as a function of the strength of the PNA pattern, the situation is less promising as far as medium range prediction is concerned. In particular, the persistence (or *regime predictability* as defined by Legras and Ghil (1985)) is rather poor. It suggests that the clusters at hand largely overlap in phase space. This implies a rapid variation of the probability to be in a particular state and therefore a rapid loss of medium range predictability. This behavior clearly highlights that the short-term predictability is not related in a simple manner to the medium range predictability of weather fields as already pointed out by Legras and Ghil (1985).

5. Toward an optimal clustering method

In Sections 3 and 4, two types of clustering have been used based, respectively, on the structural features of the underlying attractor and on some intrinsic dynamical properties of the flow. Both characteristics carry on important information on the predictability of weather fields but on different time scales. In the present section, we propose a combination of both techniques in order to build weather regimes possessing high or low sensitivity to initial conditions but keeping as far as possible the long term skill of the 3-cluster system of Section 3.

The method adopted here is to cluster the fields in two successive steps: (i) the HCA is first applied as in Section 3 and (ii) inside these clusters, one separates fields with low and high values of the K-entropy. We fix the threshold to the long term mean $K = 3.45\ \mathrm{day}^{-1}$. This approach results into 6 clusters whose anomalies are depicted in Fig. 11 and are denoted $CL_1, \ldots, CL_6$ in the following. CL_1 to CL_3 correspond to the stable regimes while CL_4 to CL_6 to the unstable regimes. Clearly, low K-entropy fields of CL_1 display a centroid with a more pronounced ridge over the rockies and a deeper low over the East pacific than the cluster C_1 (Fig. 4). This structure is reminiscent of the one associated to the positive PNA pattern. For the second cluster CL_2 corresponding to the negative PNA pattern, the positive anomalies are

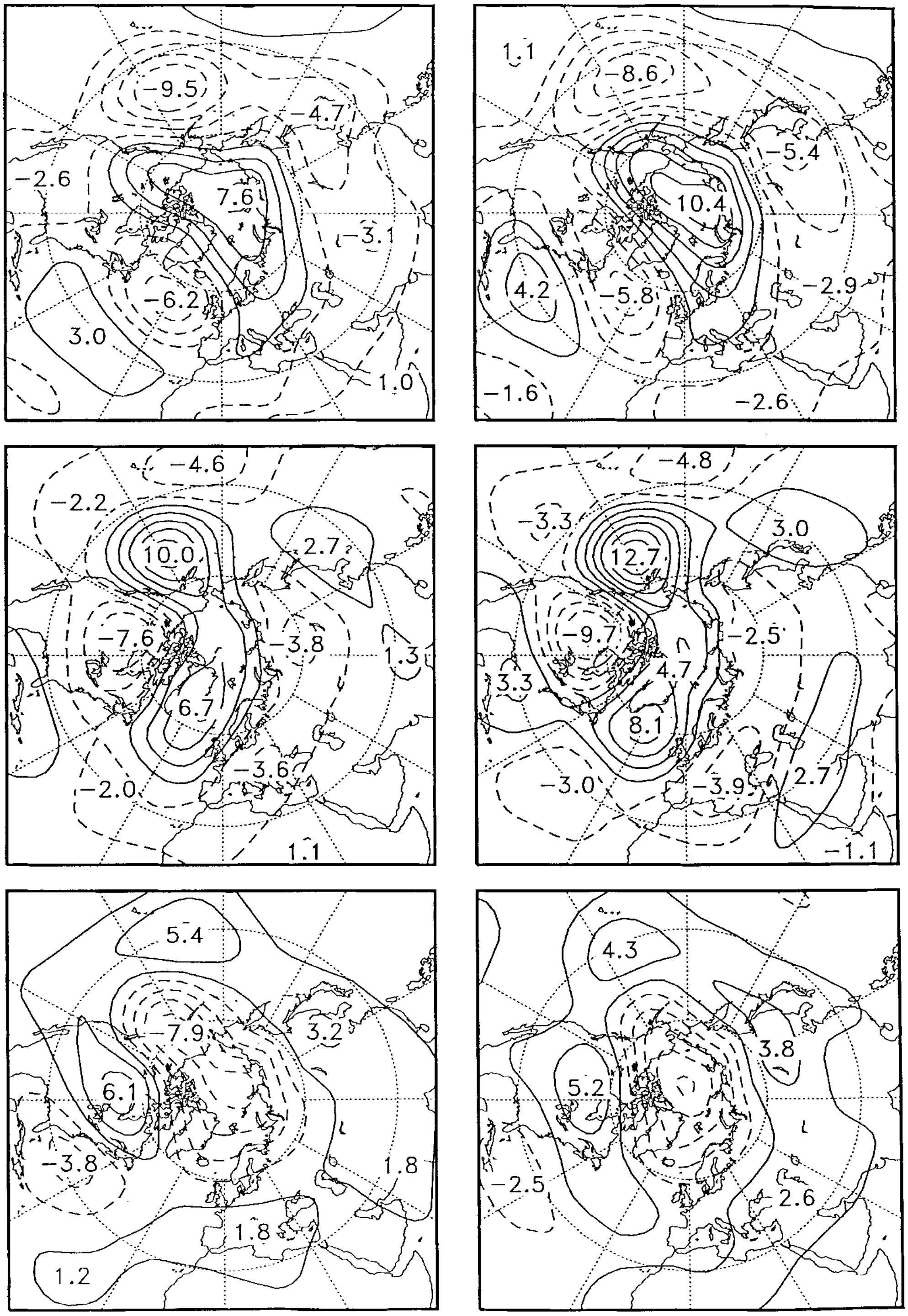

Fig. 11. Mean field anomaly (10^6 m^2/s) of the 6 clusters obtained using the combined algorithm (HCA + LA). The three stable clusters (CL_1, CL_2, CL_3 from the top to the bottom) are represented on the left while the unstable ones on the right (CL_4, CL_5, CL_6).

strengthened for unstable fields in agreement with the result of Section 4.

Let us now explore the medium range predictability of these clusters. We have first computed the two-time transition matrix of this system based on a symbolic time series of 400000 data points sampled every 3 h.

$$W = \begin{pmatrix} 0.9434 & 0.0088 & 0.0069 & 0.0401 & 0.0005 & 0.0003 \\ 0.0135 & 0.9191 & 0.0137 & 0.0009 & 0.0522 & 0.0006 \\ 0.0045 & 0.0194 & 0.9454 & 0.0002 & 0.0005 & 0.0400 \\ 0.0488 & 0.0007 & 0.0005 & 0.9319 & 0.0103 & 0.0078 \\ 0.0005 & 0.0403 & 0.0006 & 0.0130 & 0.9293 & 0.0163 \\ 0.0002 & 0.0005 & 0.0495 & 0.0034 & 0.0097 & 0.9367 \end{pmatrix}. \tag{13}$$

The large values of the diagonal elements indicate the high persistency around each cluster. The main transitions occur between states with opposite stability properties but close in phase space (from CL_1 to CL_4, CL_2 to CL_5 and CL_3 to CL_6). Note that transition from stable regions pertaining to C_1, C_2 or C_3 to the unstable regions pertaining to a different cluster is very rare, indicating that some priviledged paths exists in the dynamics.

The persistent character is confirmed by the evolution of E_{kul} plotted in Fig. 12. The slower decrease of E_{kul} than the one of Fig. 10 indicates that the long term predictability properties of these new clusters are preserved. One must also note that althougth the second and third clusters display a good short-term predictability, they present a lower skill than the other clusters on a medium range basis. Again, It stresses the absence of a clear link between short and medium range predictability.

Using the combined method proposed in this section, one is able to classify weather situations based on their short range predictability properties. Moreover, the analysis of their medium range predictability shows that they can potentially be used for medium range prediction. Note that the use of the LA clustering method does not systematically improve the medium range predictability of weather regimes as compared to the HCA technique. But one must also stress that it does not reduce their potential use for medium range prediction. Therefore, as far as predictability at short and medium ranges is concerned, this combined approach provides a promising clustering technique.

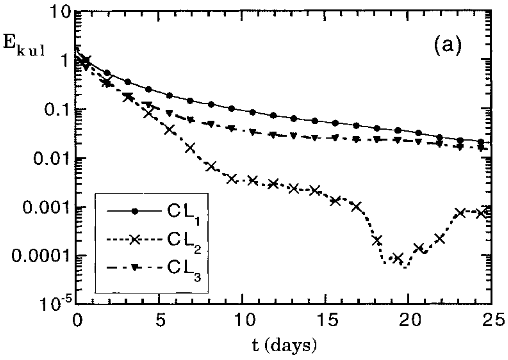

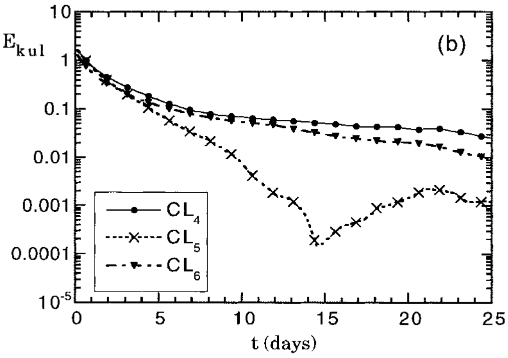

Fig. 12. Evolution of the Kullback entropy for the clusters CL_1, CL_2 and CL_3, (a), and CL_3, CL_4 and CL_5, (b), as obtained from a series of 400,000 data points sampled every 3 h.

6. Conclusions

The main idea behind weather classification is to reduce the number of possible states visited by the system in order to simplify its dynamical description. The classical procedure amounts to finding weather fields displaying similar structural features; e.g., close lying fields in the phase space of the system. Although the resulting clusters display a good medium range skill score, they do not allow for a clear distinction between weather regimes associated to highly predictable or unpredictable flows. In the present work, we have proposed a new clustering method based solely on short term instability properties of the underlying fields, namely the local Lyapunov exponents. This approach allowed us to isolate 2 regimes with opposite anomalies and displaying at the same time opposite short-term predictability properties: specifically, the cluster centroid corresponding to stable weather fields shows a strong positive PNA pattern while the cluster centroid associated to the unstable fields the opposite pattern. It appeared however that in this type of clustering, the variability of weather characteristics around each centroids is excessively large (Fig. 9) suggesting that these clusters are not well separated in phase space. As a result, the medium range skill in this case is rather poor.

The combination of both methods, the classical one and the one taking into account the values of the local Lyapunov exponents proved to be satisfactory. In particular, it yields to well separated clusters in phase space characterized by different instability properties. At the same time the method provides a cartography of the instability properties in phase space (see also Nese (1989)) and the associated predictive capability of the prevailing situation. In addition the resulting clusters keep a good skill for longer time scales as the one obtained with the classical approach (HCA).

This work can be extended in two different ways. It will be interesting to apply this approach on real data sets or in more realistic models of the atmospheric circulation in order to separate predictable and unpredictable situations on both short and medium range time scales. This analysis could be performed using the Lyapunov exponents, the singular exponents (see, e.g., Frederiksen (2000)) or a measure of the error evolution during operational forecasts. Another possibility is to develop an even more refined clustering method based on a generalized distance in a $2N$-dimensional phase space provided by both the position and the linear tendency along the trajectory. We plan to investigate further these aspects in the future.

7. Aknowledgements

We are grateful to C. Nicolis for enlightening discussions and her careful reading of the manuscript. This work is supported, in part, by the Belgian Federal Office for Scientific, Technical and Cultural Affairs under the "Pôles d'Attractions Interuniversitaires" Program P4/08.

8. Appendix A

The property of sensitivity to initial conditions is quantified through the computation of the Lyapunov exponents (Ott, 1993). In this Appendix, we summarize the computation of these quantifiers.

Consider the evolution of a nonlinear dynamical system such as the QG3 model whose fields can be described by a state vector $\boldsymbol{X}$ in a N-dimensional phase space:

$$\frac{\mathrm{d}\boldsymbol{X}}{\mathrm{d}t} = \boldsymbol{F}(\boldsymbol{X}). \tag{A.2}$$

The evolution of an infinitesimally small perturbation ($\delta\boldsymbol{x}$) is governed by the linearized evolution equation along the reference orbit $\boldsymbol{X}(t)$:

$$\frac{\mathrm{d}\delta\boldsymbol{x}}{\mathrm{d}t} = \left.\frac{\partial \boldsymbol{F}}{\partial \boldsymbol{X}}\right|_{X(t)} \delta\boldsymbol{x} \tag{A.2}$$

The solution of (A.2) can be written as,

$$\delta\boldsymbol{x}(t) = \boldsymbol{M}(t, t_0)\delta\boldsymbol{x}(t_0), \tag{A.3}$$

where $\boldsymbol{M}(t, t_0)$ is the fundamental matrix. The Lyapunov exponents are defined as the logarithm of the eigenvalues of the matrix $\boldsymbol{M}_\infty$ (Eckmann and Ruelle, 1985)

$$\boldsymbol{M}_\infty = \lim_{t\to\infty} \frac{1}{t - t_0}(M^*M)^{1/(t-t_0)}, \tag{A.4}$$

where M^* is the transpose of M. The eigenvectors of $\boldsymbol{M}_\infty$ are called the forward Lyapunov vectors (Legras and Vautard, 1995) and depends on the initial time t_0 (Goldhirsch et al., 1987). Similarly, one can define the Lyapunov exponents as the logarithm of the eigenvalue of the matrix $\boldsymbol{S}_{-\infty}$ (Legras and Vautard, 1995)

$$\boldsymbol{S}_{-\infty} = \lim_{t_0\to\infty} \frac{1}{t - t_0}(MM^*)^{1/(t-t_0)}, \tag{A.5}$$

and the eigenvectors of $\boldsymbol{S}_{-\infty}$ are called the backward Lyapunov vectors which depend on the final time t. The classical techniques used to estimate the Lyapunov exponents are based on the computation of the amplification in time of the backward Lyapunov vectors (Shimada and Nagashima, 1979). This method consists of following the evolution of a set of orthonormal vectors g_i chosen initially at random in the tangent space of the trajectory $\boldsymbol{X}(t)$. This basis is regularly orthonormalized using the standard Gram-Schmidt method to avoid the alignment of all the vectors along the most unstable direction associated to the largest Lyapunov exponent. After a rapid transient the first vector of this set, free of any constraint, will tend to the direction of maximal stretching associated to the largest Lyapunov exponent; the second vector, orthogonal to the previous one, will tend to the second most unstable direction. This set of orthonormal vectors will characterize the local directions of stretching and contraction of any perturbation and are nothing but the backward Lyapunov vectors (LVs). Their local amplifications along trajectory $\boldsymbol{X}(t)$ will give the Lyapunov exponents, σ_i as

$$\sigma_i = \lim_{\tau \to \infty} \sigma_i(\tau), \tag{A.6}$$

where

$$\sigma_i(\tau) = \frac{1}{\tau} \sum_{k=1}^{N} \ln \frac{|g_i(t_0 + k\Delta t)|}{|g_i[t_0 + (k-1)\Delta t]|}, \tag{A.7}$$

$$g_i(t_0 + k\Delta t) = M(t_0 + k\Delta t) g_i(t_0), \qquad \tau = k\Delta t. \tag{A.8}$$

If N is small, the quantity (A.7) is dependent on the position on the attractor $\boldsymbol{X}(t)$ and is called the local Lyapunov exponent which will be now written as $\sigma_i(\boldsymbol{X}, \tau)$ to indicate its phase space dependence. In the present work, we fix $N = 1$.

The local Lyapunov exponents characterize only the error amplification along a particular direction in phase space, but a typical random error can a priori grows in several directions and we are therefore faced with the growth of a volume element. To characterize this volume expansion, one usually computes the Kolmogorov–Sinai entropy (K-entropy),

$$K = \sum_{i=1}^{L^+} \sigma_i, \tag{A.9}$$

where L^+ is the number of positive Lyapunov exponents (Eckmann and Ruelle, 1985). Since we are interested here in the local properties of the flow on a non-uniform attractor, we define a local Kolmogorov entropy such that

$$K(\boldsymbol{X}, \tau) = \sum_{i=1}^{L^+} \sigma_i(\boldsymbol{X}, \tau), \tag{A.10}$$

where L^+ is the number of positive local Lyapunov values. This quantity characterizes therefore the volume expansion in the space defined by the unstable LVs.

REFERENCES

Barnston, A. B. and Livezey, R. E. 1987. Classification, seasonality and persistence of low-frequency atmospheric circulation patterns. *Mon. Weather Rev.* **115**, 1083–1126.

Cheng, X. and Wallace, J. M. 1993. Cluster analysis of the northern hemisphere wintertime 500 hPa height field: spatial patterns. *J. Atmos. Sci.* **50**, 2647–2696.

Colucci, S. J. and Baumhefner, D. P. 1992. Initial weather regimes as predictors of numerical 30-day mean forecast accuracy. *J. Atmos. Sci.* **49**, 1652–1671.

Corti, S. and Palmer, T. N. 1997. Sensitivity analysis of atmospheric low-frequency variability. *Q. J. R. Meteorol. Soc.* **123**, 2425–2447.

Déqué, M. 1988. 10-day predictability of the northern hemisphere winter 500-mb height by the ECMWF operational model. *Tellus* **40A**, 26–36.

Eckmann, J.-P. and Ruelle, D. 1985. Ergodic theory of chaos and strange attractors. *Rev. Mod. Phys.* **57**, 617–654.

Feller, W. 1971. *An introduction to probability theory and its applications*, vol. **II**, Wiley, New York.

Fraedrich, K. and Müller, K. 1982. On single station forecasting: sunshine and rainfall Markov chains. *Beitr. Phys. Atmosph.* **56**, 108–134.

Frederiksen, J. S. 1997. Adjoint sensitivity and finite-time normal mode disturbances during blocking. *J. Atmos. Sci.* **54**, 1144–1164.

Frederiksen, J. S. 2000. Singular vectors, finite time normal modes and error growth during blocking. *J. Atmos. Sci.* **57**, 312–333.

Goldhirsch, I., Sulem, P.-L. and Orszag, S. A. 1987. Stability and Lyapunov stability of dynamical systems: a differential approach and a numerical method. *Physica* **27D**, 311–337.

Hannachi, A. 1997. Weather regimes in the pacific from a GCM. Part II: dynamics and stability. *J. Atmos. Sci.* **54**, 1334–1348.

Hannachi, A. and Legras, B. 1995. Simulated annealing and weather regimes classification. *Tellus* **47A**, 955–973.

Kimoto M., Mukougawa, M. and Yoden, S. 1992. Medium range forecast skill variation and blocking transition: a case study. *Mon. Wea. Rev.* **120**, 1616–1627.

Lasota, A. and Mackey, M. 1995. *Chaos, fractals and noise: stochastic aspects of the dynamics.* Springer-Verlag, New-York, 472 p.

Legras, B. and Ghil, M. 1985. Persistent anomalies, blocking and variations in atmospheric predictability. *J. Atmos. Sci.* **42**, 433–471.

Legras, B. and Vautard, R. 1995. A guide to Lyapunov vectors. ECMWF Seminar Proceedings. *Predictability*, vol. **I**, 143–156.

Lin, H. and Derome, J. 1996. Changes in predictability associated with the PNA pattern. *Tellus* **48A**, 553–571.

Marshall, J. and Molteni, F. 1993. Toward a dynamical understanding of planetary-scale flow regimes. *J. Atmos. Sci.* **50**, 1792–1818.

Molteni, F., Tibaldi, S. and Palmer, T. N. 1990. Regimes in the wintertime circulation over northern extratropics. (I) Observational evidence. *Q. J. R. Meteorol. Soc.* **116**, 31–67.

Molteni F. and Palmer, T. N. 1993. Predictability and finite-time instability of the northern winter circulation. *Quart. J. Roy. Meteor. Soc.* **119**, 269–298.

Molteni, F., Buizza, R., Palmer, T. N. and Petroliagis, T. 1996. The ECMWF ensemble prediction system: methodology and validation. *Q. J. R. Meteorol. Soc.* **122**, 73–119.

Nese, J. M. 1989. Quantifying local predictability in phase space. *Physica D* **35**, 237–250.

Nicolis, C., Ebeling and Baraldi, C. 1997. Markov processes, dynamic entropies and the statistical prediction of mesoscale weather regimes. *Tellus* **49A**, 108–118.

Nicolis C. and Nicolis, G. 1995. Chaos in dissipative systems: understanding atmospheric physics. *Adv. Chem. Phys.* **XCI**, 511–570.

Ott, E. 1993. *Chaos in dynamical systems.* Cambridge University Press.

Palmer, T. N. 1988. Medium and extended range predictability and stability of the Pacific/North American mode. *Q. J. R. Meteorol. Soc.* **114**, 691–713.

Shimada, I. and Nagashima, T. 1979. A numerical approach of dissipative dynamical systems. *Prog. Theor. Phys.* **61**, 1605–1616.

Spekät, A., Heller-Schulze, B. and Lutz, M. 1983. Üeber Grosswetter und Markov-Ketten. *Meteor. Rundsch.* **36**, 243–248.

Toth, Z. and Kalnay, E. 1997. Ensemble forecasting at NCEP and the breeding method. *Mon. Wea. Rev.* **125**, 3297–3319.

Trevisan, A. 1995. Statistical properties of predictability from atmospheric analogs and the existence of multiple flow regimes. *J. Atmos. Sci.* **52**, 3577–3592.

Vannitsem, S. and Nicolis, C. 1997. Lyapunov vectors and error growth patterns in a T21L3 quasi-geostrophic model. *J. Atmos. Sci.* **54**, 347–361.

Vannitsem, S. and Nicolis, C. 1998. Fine-scale variables versus averaged observables in a T21L3 quasi-geostrophic model. *Q. J. R. Meteorol. Soc.* **125**, 2201–2226.

Wallace J. M. and Gutzler, D. S. 1981. Teleconnections in the geopotential height field during the northern hemisphere winter. *Mon. Weather Rev.* **109**, 784–812.

Ward, J. 1963. Hierarchical grouping to optimize an objective function. *J. Amer. Stat. Soc.* **58**, 236–244.